Synchronous dynamics in the presence of short-term plasticity

Matteo di Volo,[1,2,*] Roberto Livi,[2,3,4,5,†] Stefano Luccioli,[2,4,5,‡] Antonio Politi,[2,4,6,§] and Alessandro Torcini[2,4,5,‖]

[1]*Department of Physics, Università degli Studi di Parma, via G.P. Usberti 7/A, I-43124 Parma, Italy*

[2]*Centro Interdipartimentale per lo Studio delle Dinamiche Complesse, Università di Firenze, via G. Sansone 1, I-50019 Sesto Fiorentino, Italy*

[3]*Department of Physics, Università di Firenze, via G. Sansone 1 - I-50019 Sesto Fiorentino, Italy*

[4]*CNR - Consiglio Nazionale delle Ricerche, Istituto dei Sistemi Complessi, via Madonna del Piano 10, I-50019 Sesto Fiorentino, Italy*

[5]*Istituto Nazionale di Fisica Nucleare, Sezione di Firenze, via G. Sansone 1 - I-50019 Sesto Fiorentino, Italy*

[6]*Institute for Complex Systems and Mathematical Biology and Scottish Universities Physics Alliance, University of Aberdeen, Aberdeen AB24 3UE, United Kingdom*

(Received 11 December 2012; published 4 March 2013)

We investigate the occurrence of quasisynchronous events in a random network of excitatory leaky integrate-and-fire neurons equipped with short-term plasticity. The dynamics is analyzed by monitoring both the evolution of global synaptic variables and, on a microscopic ground, the interspike intervals of the individual neurons. We find that quasisynchronous events are the result of a mixture of synchronized and unsynchronized motion, analogously to the emergence of synchronization in the Kuramoto model. In the present context, disorder is due to the random structure of the network and thereby vanishes for a diverging network size N (i.e., in the thermodynamic limit), when statistical fluctuations become negligible. Remarkably, the fraction of asynchronous neurons remains strictly larger than zero for arbitrarily large N. This is due to the presence of a robust homoclinic cycle in the self-generated synchronous dynamics. The nontrivial large-N behavior is confirmed by the anomalous scaling of the maximum Lyapunov exponent, which is strictly positive in a finite network and decreases as $N^{-0.27}$. Finally, we have checked the robustness of this dynamical phase with respect to the addition of noise, applied to either the reset potential or the leaky current.

DOI: 10.1103/PhysRevE.87.032801 PACS number(s): 84.35.+i, 05.45.Xt, 87.19.L−

I. INTRODUCTION

The spontaneous emergence of synchronization phenomena in neural dynamics is a widely investigated and debated issue. Many experimental studies have pointed out the importance of such dynamical regimes both *in vitro* and *in vivo* (see, e.g., Ref. [1]). They have also triggered the introduction of several mathematical models to understand the basic mechanisms. Many different ingredients have been invoked to obtain a reasonable correspondence with the experimental observations. Tsodyks, Uziel, and Markram [2] invoke short-term plasticity as a possible source of quasisynchronous events in the form of population bursts (PBs) in a neural network of leaky integrate-and-fire (LIF) neurons with inhibitory and excitatory couplings. The system studied by these authors, besides accounting for short-term plasticity (as in the seminal works in Refs. [3,4]), includes various forms of quenched disorder: (i) random dilution with a given ratio of excitatory and inhibitory neurons, (ii) a Gaussian distribution of the coupling strengths and of the synaptic time scales, and (iii) random leaky currents (uniformly distributed). Still, the predictions have remained quantitatively far from the experimental findings. A step forward was made by Volman *et al.* [1], who studied a modified version of the previous model: LIF neurons were replaced by Morris-Lecar ones [5], global coupling was assumed (maintaining the same ratio of inhibitory and excitatory neurons), and a noise term was added to the leaky current. In fact, these modifications proved successful in reproducing the long tail distribution of the time intervals between successive PBs, observed in the experiments. Later, PBs were consistently found in a similar model for different network topologies (i.e,, random, nearest neighbors, and modular) [6]. More recently, Chen and Jasnow [7] reconsidered the model of Ref. [2] in a fully coupled network of excitatory neurons in the presence of additive noise. By transforming the continuous-time dynamics into an event-driven map [8], they observed a dynamical regime where high- and low-activity regimes alternate in time: The sporadic asynchronous neural activity is mainly due to the stochastic component of the dynamics. Finally, in Ref. [9], partially synchronized states were investigated in a balanced neural network by invoking a different plasticity mechanism.

Since it is desirable to understand the role played by each ingredient, here we investigate the occurrence of quasisynchronized events (QSEs) in a minimal model of excitatory LIF neurons with short-term plasticity (as defined in Ref. [3]). We start by studying the dynamics of fully coupled networks, finding that the evolution converges to a completely synchronized dynamics, and then move on to randomly diluted networks, in which context QSEs emerge as a result of a mixed behavior: Neurons split into locked and unlocked neurons. Since this scenario is reminiscent of the emergence of synchronization in ensembles of phase oscillators, we have explored possible relationships with standard models. For various reasons, the analogy with the Kuramoto model cannot be pushed too far [in particular since the fully synchronized regime should emerge already for a finite N (see below)]. The neural network with exponentially shaped postsynaptic pulses studied by Tsodyks Mitkov, and Sompolinsky [10] turns out to be a much more appropriate reference model since there

*matteo.divolo@fis.unipr.it
†livi@fi.infn.it
‡stefano.luccioli@fi.isc.cnr.it
§a.politi@abdn.ac.uk
‖alessandro.torcini@cnr.it

(like in the present setup) the synchronous solution belongs to a homoclinic cycle, so that an arbitrarily small amount of noise can drive the solution away from the synchronized state. It is interesting to note that such a type of marginally stable solution is spontaneously generated by the dynamical system rather than being the result of some *ad hoc* parameter adjustment.

In Sec. II we introduce the model and its reduction to an event-driven map. Section III is devoted to a general discussion of the dynamical properties. In particular we estimate the Lyapunov exponents, finding evidence of a chaotic dynamics, and that chaos tends to disappear when the number N of neurons diverges. More precisely, the maximum exponent decreases as $N^{-0.27}$. Section IV is devoted to a detailed analysis of QSEs that are characterized with the help of suitable collective variables that measure the synaptic activity. We study also the dependence of the fraction f_u of unlocked neurons on the network size, finding that it decreases quite slowly, namely, $f_u \approx N^{-0.1}$. In Sec. V we discuss the robustness of the QSE phase with respect to the addition of noise. In particular we consider a noise acting on (i) the reset potential and (ii) the leaky current. In both cases, QSEs survive the addition of relatively large noise amplitudes, confirming that random dilution of the network and short-term plasticity provide a robust setup for the sustainment of the QSE phase in a network of excitatory LIF neurons. Conclusions and open problems are presented in Sec. VI. Finally, the Appendix is devoted to the stability analysis of the synchronous solution.

II. MODEL

In this paper we consider a network of N excitatory LIF neurons interacting via a synaptic current and regulated by short-term plasticity according to a model introduced in Ref. [3]. The membrane potential V_j of each neuron evolves in time according to the differential equation

$$\tau_m \dot{V}_j = E_c - V_j + R_{\rm in} I_{\rm syn}(j), \tag{1}$$

where τ_m is the membrane time constant, $R_{\rm in}$ is the membrane resistance, $I_{\rm syn}(j)$ is the synaptic current received by neuron j from all its presynaptic neurons (see below for its mathematical definition), and E_c is the contribution of a constant external current (properly multiplied by the resistance $R_{\rm in}$).

Whenever the potential $V_j(t)$ reaches the threshold value $V_{\rm th}$, it is reset to V_r and a spike is sent towards the postsynaptic neurons. For the sake of simplicity the spike is assumed to be a δ-like function of time. Accordingly, the spike train $S_j(t)$ produced by neuron j is defined as

$$S_j(t) = \sum_m \delta(t - t_j(m)), \tag{2}$$

where $t_j(m)$ is the time when neuron j fires its mth spike.

The transmission of the field S_j is mediated by the synapse dynamics. For the sake of simplicity we assume that all efferent synapses of a given neuron follow the same evolution (this is justified insofar as we assume that no inhibitory coupling is present). Moreover, by following Ref. [2], the state of the ith synapse is assumed to be characterized by three variables x_i, y_i, and z_i, which represent the fractions of synaptic transmitters in the recovered, active, and inactive states, respectively ($x_i + y_i + z_i = 1$). The evolution equations are

$$\dot{y}_i = -\frac{y_i}{\tau_{\rm in}} + u x_i S_i, \tag{3}$$

$$\dot{z}_i = \frac{y_i}{\tau_{\rm in}} - \frac{z_i}{\tau_r}. \tag{4}$$

Only the active transmitters react to the incoming spikes S_i: The parameter u tunes their effectiveness. Moreover, $\tau_{\rm in}$ is the characteristic decay time of the postsynaptic current, while τ_r is the recovery time from synaptic depression. For the sake of simplicity, we assume that all parameters appearing in the above equations are independent of the neuron indices. The model equations are finally closed, by representing the synaptic current as the sum of all the active transmitters delivered to neuron j,

$$I_{\rm syn}(j) = \frac{G}{N} \sum_{i \neq j} \epsilon_{ij} y_i, \tag{5}$$

where G is the strength of the synaptic coupling (which we assume independently of both i and j) and ϵ_{ij} is the connectivity matrix whose entries are set equal to 1 or 0 if the presynaptic neuron i is connected to or disconnected from the postsynaptic neuron j, respectively. Since we assume that the input resistance $R_{\rm in}$ is independent of j, it can be included in G. In this paper we study the case of excitatory coupling between neurons, i.e., $G > 0$. Moreover, we assume that each neuron is connected to a macroscopic number $O(N)$ of presynaptic neurons: This is the reason why the sum is divided by the factor N. This makes transparent that a nontrivial dynamics can be observed for a coupling constant of order $1/N$. Typical values of the parameters contained in the model have a phenomenological origin [2,6]. In the following, unless otherwise stated, we use the following set of values: $\tau_{\rm in} = 6$ ms, $\tau_m = 30$ ms, $\tau_r = 798$ ms, $V_r = 13.5$ mV, $V_{\rm th} = 15$ mV, $E_c = 15.45$ mV, $G = 45$ mV, and $u = 0.5$. Numerical simulations of the model can be worked out much more effectively by introducing the dimensionless quantities

$$a = \frac{E_c - V_r}{V_{\rm th} - V_r}, \tag{6}$$

$$g = \frac{G}{V_{\rm th} - V_r}, \tag{7}$$

$$v = \frac{V - V_r}{V_{\rm th} - V_r} \tag{8}$$

and rescaling time and all the other temporal parameters with the membrane time constant τ_m (for simplicity we keep the notation unchanged also after rescaling). The values of the rescaled parameters are $\tau_{\rm in} = 0.2$, $\tau_r = 133\tau_{\rm in}$, $v_r = 0$, $v_{\rm th} = 1$, $a = 1.3$, $g = 30$, and $u = 0.5$. While the rescaled Eqs. (3) and (4) keep the same form, Eq. (1) changes to

$$\dot{v}_j = a - v_j + \frac{g}{N} \sum_{i \neq j} \epsilon_{ij} y_i. \tag{9}$$

A major advantage for numerical simulations comes from the possibility of transforming the set of differential equations (3), (4), and (9) into an event-driven map [8,11]. In fact, these differential equations can be formally integrated from time t_n to time t_{n+1}, where t_n is the instant of time

immediately after the nth spike in the network.[1] The resulting map for neuron i reads

$$z_i(n+1) = z_i(n)e^{-\tau(n)/\tau_r} + \frac{\tau_r}{\tau_r - \tau_{\rm in}} y_i(n)(e^{-\tau(n)/\tau_r} - e^{-\tau(n)/\tau_{\rm in}}), \quad (10)$$

$$v_i(n+1) = v_i(n)e^{-\tau(n)} + a(1 - e^{-\tau(n)}) + gF_i(n), \quad (11)$$

$$y_i(n+1) = y_i(n)e^{-\tau(n)/\tau_{\rm in}} + u\left[1 - \frac{\tau_r}{\tau_r - \tau_{\rm in}} y_i(n)\left(e^{-\tau(n)/\tau_r} - \frac{\tau_{\rm in}e^{-\tau(n)/\tau_{\rm in}}}{\tau_r}\right) - z_i(n)e^{-\tau(n)/\tau_r}\right]\delta_{i,s}, \quad (12)$$

where the index s refers to the neuron spiking at time t_{n+1}, $\tau(n) = t_{n+1} - t_n$ is the nth interspike interval (ISI) in the network, and $F_i(n)$ has the expression

$$F_i(n) = \frac{\tau_{\rm in}}{\tau_{\rm in} - 1}(e^{-\tau(n)/\tau_{\rm in}} - e^{-\tau(n)})\frac{1}{N}\sum_{j\neq i}\epsilon_{ji}y_j(n), \quad (13)$$

with the sum running over the index j of all presynaptic neurons of neuron i. Notice that $\tau(n)$ can be determined by computing the time

$$\tau_i(n) = \ln\left[\frac{a - v_i(n)}{a + gF_i(n) - 1}\right], \quad i = 1, \ldots, N \quad (14)$$

needed by the ith neuron to reach the threshold value and thereby selecting the shortest one

$$\tau(n) = \inf_i\{\tau_i(n) | i = 1,2,\ldots,N\}.$$

III. DYNAMICS

The deterministic model with short-term plasticity described in the preceding section contains minimal ingredients with respect to the models mentioned in the Introduction. In fact, the event-driven dynamics described by Eqs. (10)–(12) is governed by four parameters, namely, $\tau_{\rm in}$, τ_r, a, and g. In what follows we mostly explore the role of $\tau_{\rm in}$ while keeping constant the phenomenological ratio $\tau_r/\tau_{\rm in} = 133$.

Numerical simulations show that in the fully coupled case ($\epsilon_{ij} = 1\ \forall i,j$), generic initial conditions always converge towards a synchronized regime with all neurons firing simultaneously. This is a standard scenario that can be observed in many networks of identical fully coupled phase oscillators. In particular, the same behavior is found in networks without plasticity when the transmitted pulse has an infinitely fast rise time, e.g., exponential or δ pulses [12,13]. Notice that the event-driven algorithm in Eqs. (10)–(12) has to be suitably modified in order to remove the ambiguities that emerge when the synchronous state is approached: Because of the finite computer precision, the identification of the firing neuron may not yield a unique index. This problem can be straightforwardly overcome by reducing the dynamics of the synchronized neurons to that of a single one.

The stability of this regime can be assessed by determining the evaporation exponent Λ [14], i.e., the convergence rate of a hypothetical single neuron that is subject to the mean field generated by the network. The analysis carried out in the Appendix reveals a rather awkward property, namely, that the solution is stable against negative perturbations and unstable otherwise (see the left and right exponents in Fig. 12). This is because the periodic solution selected by the network belongs to a homoclinic cycle that is obtained from the collapse of a stable solution with an unstable one. This property was already proved in Ref. [10] with reference to the Tsodyks-Mitkov-Sompolinsky (TMS) model in the absence of synaptic plasticity. In our model, one can apply the same mathematical formalism since the synchronized regime is characterized by a sequence of exponential pulses. In the case of a fully coupled network, the asymmetric stability of the synchronous regime has no relevant consequences since the neurons that possibly escape while being ahead of the cluster are eventually attracted when they approach the cluster from the opposite side. We will see that this property has instead relevant consequences as soon as disorder is added to the network.

A second remarkable property is that the synchronized state is stable for all parameter values and Λ remains finite even in the limit $\tau_{\rm in} \to 0$, when the coupling vanishes. In fact, when the synaptic time scales $\tau_{\rm in}$ and τ_r are significantly smaller than the typical ISI, the active transmitter variable $y_i(t)$ exhibits a short pulse (of finite height and duration $\tau_{\rm in}$) so that the membrane potential of all connected neurons increases by an amount

$$\Delta v_i(n) = g\tau_{\rm in}e^{-\tau(n)}\frac{u}{N},$$

which evidently vanishes for $\tau_{\rm in} \to 0$. As shown technically in the Appendix, the synchronized state is nevertheless characterized by a finite stability because it is surrounded by a tiny basin of attraction (of size $\tau_{\rm in}$). As a result, this model does not reduce for $\tau_{\rm in} \to 0$ to a standard LIF network with δ pulses [11] and the stability of the synchronized state differs by a finite amount.

After having discussed the dynamics of the fully coupled network, we now study the effect of quenched disorder. We consider a diluted network made of N neurons with a finite fraction of broken directed links. In practice, we design such a diluted network by connecting each directed pair of neurons with probability p (notice that if the presynaptic neuron i is connected to the postsynaptic neuron j, this does not imply that j is also a presynaptic neuron of i). This corresponds to a directed Erdős-Renyi (ER) network where the average connectivity $\langle c\rangle = pN$ is an extensive quantity (in this article we have always considered $p = 0.7$). This is consistent with the normalization of the coupling term in Eq. (9). The indicators used to characterize the resulting dynamics have

[1] In the time interval immediately after the last spike of the network, at time t_n, and before the emission of the next one, at time t_{n+1}, all the variables y_i evolve as $y_i^-(n+1) = y_i(n)\exp[-\tau(n)/\tau_{\rm in}]$ [according to Eq. (3), without the source term ux_iS_i]. Then, at time t_{n+1}, the variable y_s corresponding to the neuron s, the one reaching the threshold at that time, is subject to a kick $u(1 - y - z)$. The complete updating rule for the variables y_i reads $y_i(n+1) = y_i^-(n+1) + u[1 - y_i^-(n+1) - z_i(n+1)]\delta_{i,s}$, where $z_i(n+1)$ is obtained by integrating Eq. (4) with $y_i = y_i(n)\exp(-t/\tau_{\rm in})$. Finally, the updating rule for the variables v_i is obtained by integrating Eq. (9) with $y_i = y_i(n)\exp(-t/\tau_{\rm in})$.

been averaged over different realizations of the quenched disorder.

It is instructive to characterize the network dynamics by monitoring the Kuramoto parameter [15]

$$R = \left\langle \left| \frac{1}{N} \sum_i e^{i\theta_i} \right| \right\rangle, \tag{15}$$

$$\theta_i(t,m) = 2\pi \frac{t - t_i(m)}{t_i(m+1) - t_i(m)}, \tag{16}$$

where $\langle\,\rangle$ denotes a time average and $\theta_i(t,m)$ is the phase of neuron i at time $t \in [t_i(m), t_i(m+1)]$.

In Fig. 1(a) we plot the Kuramoto parameter R versus the decay time $\tau_{\rm in}$ for a network with 500 neurons (see the bottom curve). For $\tau_{\rm in} \to 0$, the evolution is perfectly synchronous ($R = 1$), but upon increasing $\tau_{\rm in}$, the degree of synchrony is progressively lost until an almost asynchronous regime sets in (for $\tau_{\rm in} >\approx 1$). The raster plots obtained for different parameter values see Figs. 1(b)–1(d)] help to visualize the underlying dynamics. In particular, we see that synchrony manifests itself as sharp QSEs for $\tau_{\rm in} = 0.2$, which spread in time when $\tau_{\rm in}$ is increased and eventually disappear for $\tau_{\rm in} = 1.2$. In the last regime, the average value of the ISI of each neuron i, $\langle {\rm ISI}_i \rangle$, is distributed according to a Gaussian with a small variance (see Fig. 2).

The overall scenario is reminiscent of the Kuramoto synchronization transition in an ensemble of globally coupled oscillators when either the disorder is progressively increased or the coupling constant is decreased [16]. In fact, in the $N \to \infty$ limit, massively coupled Erdős-Renyi networks such as those we have studied here are indistinguishable from globally coupled oscillators [the only difference being a reduced coupling strength, by a factor p (see Ref. [17])]. For finite N, the diversity in the connectivities of the single neurons represents a source of disorder that may be strong enough to destroy the synchronized state. What is to be understood is the reason why the coherence is lost upon increasing $\tau_{\rm in}$, as the disorder does not change. The evaporation exponent Λ determined in the Appendix tells us that the progressive loss of coherence is to be attributed to the weaker stability of the synchronized state when $\tau_{\rm in}$ is progressively increased. Moreover, the top curve in Fig. 1(a), obtained for $N = 5000$, confirms that in a larger network, a higher degree of synchronization is observed as a consequence of the smaller effective disorder.

We have completed the numerical study of the stability properties by computing the Lyapunov exponents of the network in the presence of QSEs. In Fig. 3(a) we show the spectrum of the Lyapunov exponents in a network of $N = 50$ neurons for the phenomenological value $\tau_{\rm in} = 0.2$. There exists a small positive component, as can be appreciated from the inset, which reveals the chaotic nature of the dynamics. More precisely, the Kaplan-Yorke dimension is approximately equal to 12, i.e., we are facing a very thin attractor embedded in a configuration space of much higher dimension. The chaotic nature of the evolution is not at all surprising given the nonlinear (or, better, the piecewise linear) character of the model. In contrast, in the thermodynamic limit, since the dynamics reduces to a strictly periodic evolution, one expect chaos to disappear. In fact, as shown in Fig. 3(b),

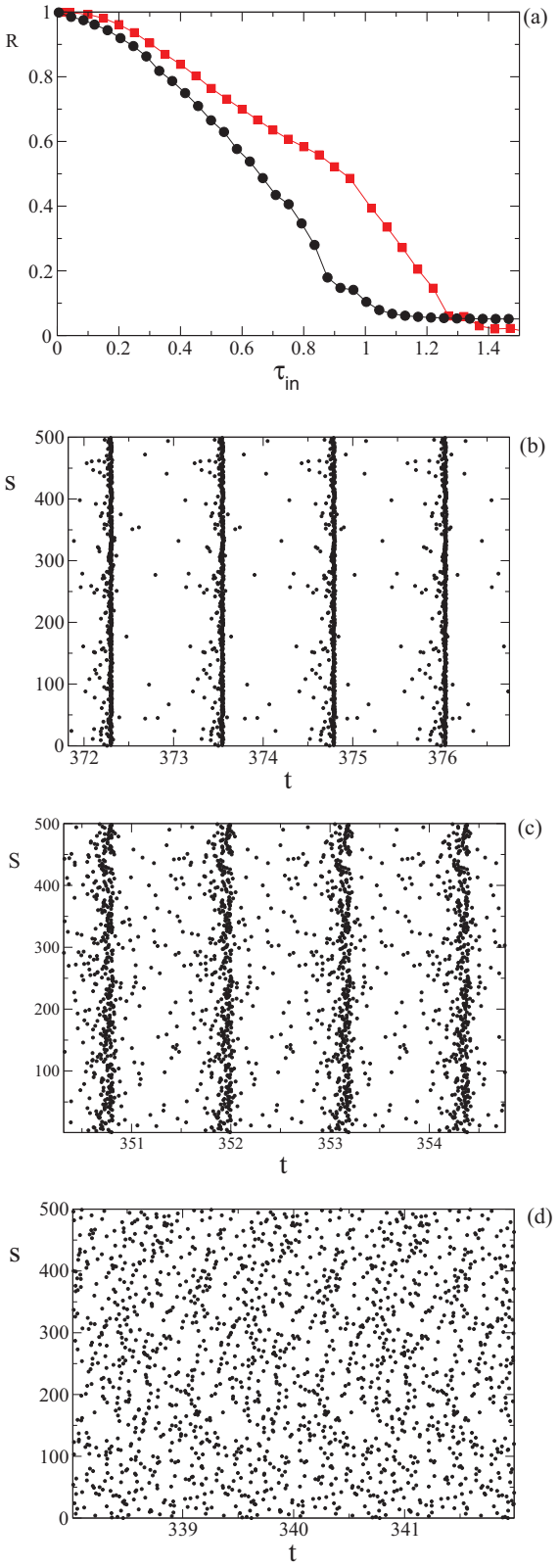

FIG. 1. (Color online) (a) Kuramoto order parameter R as a function of $\tau_{\rm in}$ for a diluted network with $N = 500$ (black circles) and $N = 5000$ (red squares). The values of R have been obtained by averaging over a temporal length of 40 000 after discarding a transient of $1000N$ iterations of the map. In (b)–(d) we report the firing patterns for $\tau_{\rm in} = 0.2, 0.5$, and 1.2, respectively; s is the index of the neuron firing at time t.

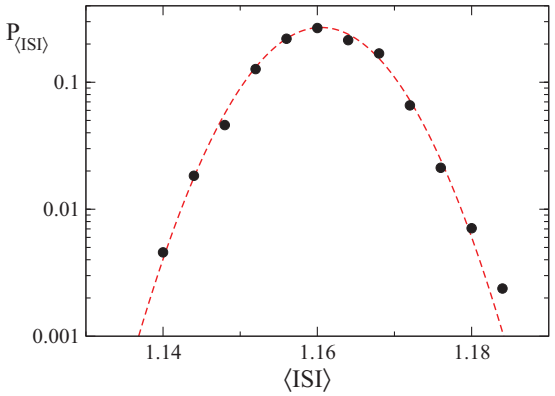

FIG. 2. (Color online) Probability distribution of ⟨ISI⟩ for a diluted network with $N = 500$ in the asynchronous dynamical phase ($\tau_{in} = 1.2$). Data have been obtained after discarding a transient of $1000N$ iterations of the map and by sampling 1000 ISI values for each neuron. The dashed line is a Gaussian fit with average $\langle ISI \rangle \simeq 1.16$ and standard deviation $\sigma \sim O(10^{-2})$.

the maximum Lyapunov exponent λ_1 vanishes in the limit $N \to \infty$. This is consistent with previous studies in the absence of synaptic plasticity (see, e.g., Ref. [17]), although the convergence here is significantly slower, $\lambda_1 \propto N^{-\delta}$ with $\delta = 0.27 \pm 0.01$ instead of $\delta = 1/2$, as expected on the basis of simple statistical arguments. A similar slow convergence was observed in Ref. [18], where it can be traced back to the network structure that is not so massively connected. The slow rate observed herein is presumably related to the anomalous number of nonsynchronized neurons (see the following section and Sec. VI).

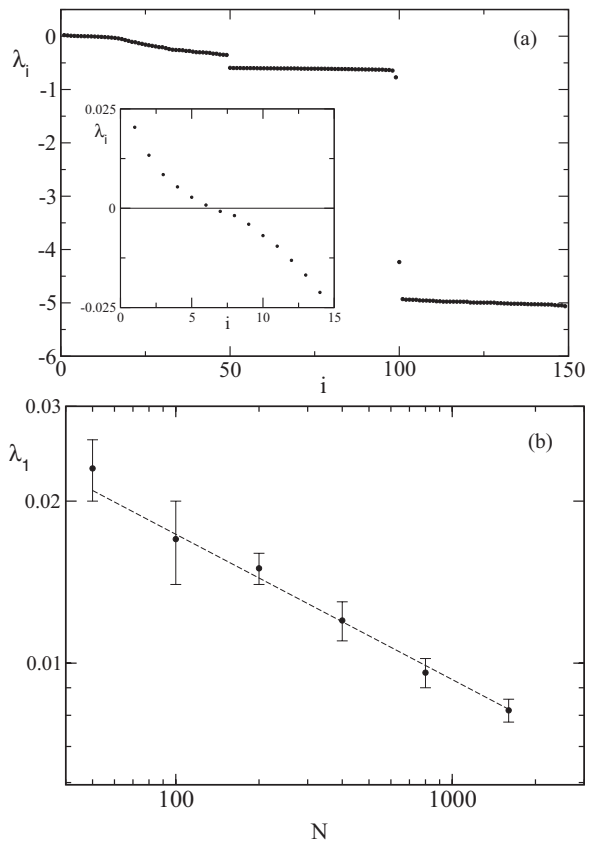

FIG. 3. (a) Spectrum of Lyapunov exponents, labeled according to the natural ordering, for a diluted network of size $N = 50$. The inset shows a close-up of the spectrum to show the presence of six positive exponents. (b) Maximum Lyapunov exponent λ_1 as a function of the number of neurons N: The measures of λ_1 have been averaged over ten different realizations of the network (the error bars refer to the maximum deviation from the average). A power-law fit is reported (dashed line) with decay exponent $\delta = 0.27 \pm 0.01$. In both cases we have considered $\tau_{in} = 0.2$.

IV. QUASISYNCHRONIZED EVENTS

In this section we closely investigate the QSE phase for the phenomenological value $\tau_{in} = 0.2$. From the raster plot shown in Fig. 1(b), we can see that QSEs alternate almost regularly with time spans characterized by a highly reduced neural activity. A closer look shows that the neuron spikes are not exactly synchronized within the QSEs; this is consistent with the evidence given in the preceding section of a microscopic chaotic dynamics. In order to characterize the collective evolution of the QSEs, it is convenient to represent the average synaptic fields in terms of suitable global observables

$$Y(t) = \frac{1}{N}\sum_{i=1}^{N} y_i(t), \quad Z(t) = \frac{1}{N}\sum_{i=1}^{N} z_i(t). \tag{17}$$

The resulting phase portrait is plotted in Fig. 4: The almost perfect closed curve confirms the periodic character of the collective motion. The evidence of the microscopic chaos manifests itself as a finite tiny width of the line. A quantitative analysis can be performed by looking at the distribution $P(T_q)$ of the time intervals T_q between two consecutive QSEs (defined as the separation between two maxima of the global activity Y). In Fig. 5 we can see that $P(T_q)$ has a clean Gaussian shape.

At the microscopic level, QSEs are generated by essentially the same macroscopic number of neurons that are locked to the QSEs, while the remaining unlocked neurons contribute, most of the time, to the sporadic neural activity and occasionally to QSEs. In Fig. 6(a) we plot the microscopic phase portrait of a locked and an unlocked neuron by reporting one ISI versus the previous one. The return map of the locked neuron consists of small fluctuations around a single point, while that of the unlocked neuron reveals an essentially quasiperiodic dynamics.

One could argue that the major reason for the different behavior exhibited by the single neurons is their connectivity since a larger connectivity increases the spiking frequency. In Fig. 6(b) we show the average interspike interval $\langle ISI_i \rangle$ of each neuron as a function of its excess connectivity $\tilde{c}_i = (c_i - \langle c \rangle)/\sigma$, where $\sigma = \sqrt{\langle c^2 \rangle - \langle c \rangle^2} = \sqrt{Np(1-p)}$ and $\langle c \rangle = pN$ locked neurons are recognized as such since the corresponding $\langle ISI_i \rangle$ is independent of i. They are typically characterized by a negative excess connectivity $\tilde{c}$. Conversely, the average ISI of the unlocked neurons covers a range of different values. Moreover, there exists a borderline interval of positive $\tilde{c}$ values (close to $\tilde{c} = 0$), where both groups are simultaneously present. Altogether, this scenario is quite similar to the one arising in the usual Kuramoto model, when the coupling is strong enough to synchronize the

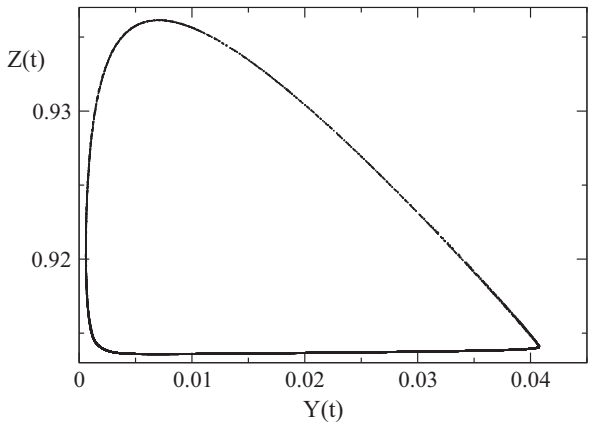

FIG. 4. Global attractor of the QSE dynamical phase represented by the average synaptic fields $Y(t)$ and $Z(t)$ for $N = 10\,000$ and $\tau_{in} = 0.2$. Data are reported after discarding a transient of $1000N$ iterations of the map.

sufficiently resonant oscillators, while all the others remain unsynchronized. There are, however, differences: Here (i) the coupling affects the spiking frequency, so it is less straightforward to determine those neurons that are involved in the synchronized motion and (ii) the disorder is not in the single-neuron dynamics (all neurons are identical) but follows from the diversity of the connections.

On a quantitative level, numerical simulations indicate that the number N_u of unlocked neurons grows as N^η with $\eta = 0.90 \pm 0.01$ [see Fig. 7(a)], so the fraction f_u of unlocked neurons decreases as $N^{-0.1}$. It is remarkable to see that f_u does not drop to zero for a finite N. In fact, statistical arguments tell us that the amount of disorder (which manifests itself as a variable connectivity) is expected to vanish as $1\sqrt{N}$ and should

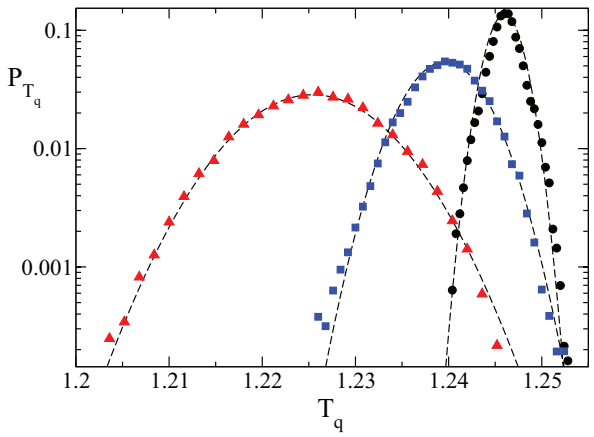

FIG. 5. (Color online) Probability distribution of T_q for the deterministic dynamics (black circles), the stochastic dynamics with noise on the leaky current (blue squares), and the stochastic dynamics with noise on the reset potential (red triangles). Distributions have been obtained for a diluted network with $N = 500$ and $\tau_{in} = 0.2$ by discarding a transient of $1000N$ iterations of the map and sampling $10\,000$ T_q values. The distributions have been fitted with Gaussian curves (see the dashed lines) with averages $\langle T_q \rangle = 1.246$, 1.239, and 1.226, respectively, and standard deviations $\sigma = 1.7 \times 10^{-3}$, 4.0×10^{-3}, and 7.0×10^{-3}, respectively. For both cases of stochastic dynamics $\Delta = 0.1$ (see Sec. V).

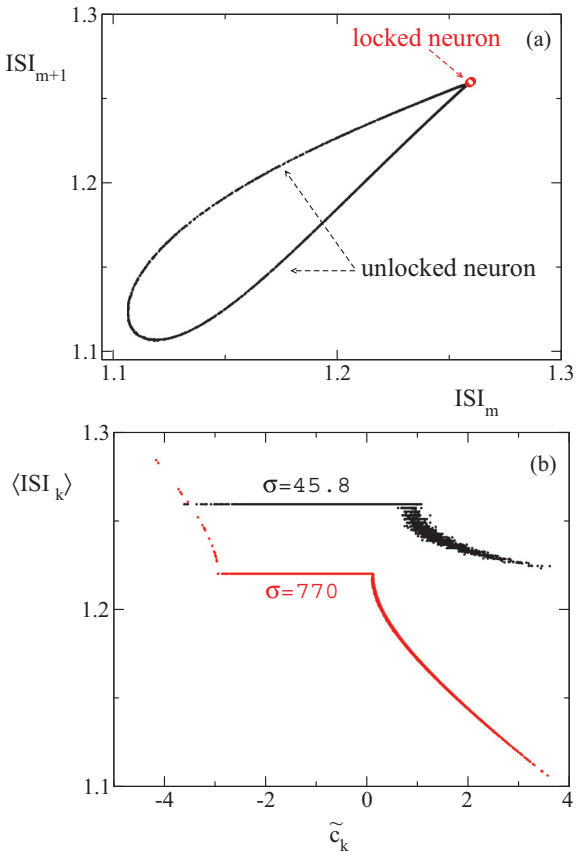

FIG. 6. (Color online) (a) The ISI return map for a locked neuron with $c - \langle c \rangle = -2$ (red open circles) and an unlocked neuron with $c - \langle c \rangle = 117$ (black dots) (data have been collected in the same simulation of Fig. 4). (b) The $\langle \mathrm{ISI}_k \rangle$ for all $k = 1, \ldots, N$ neurons as a function of their normalized connectivity $\tilde{c}_k$ for two different topologies of diluted networks with the same size $N = 10\,000$ and the same $\langle c \rangle = pN$. The top curve (black dots) refers to an ER network with $\sigma = \sqrt{Np(1-p)} = 45.8$. The bottom curve (red dots) refers to a different network with a much higher standard deviation $\sigma = 770$ (see the text for details). Averages have been obtained by sampling $10\,000$ firing events for each neuron after discarding a transient of $10\,000N$ iterations of the map. The parameter $\tau_{in} = 0.2$ is the same for both networks.

therefore become, at some point, smaller than the barrier height of the valley that contains the synchronous solution. This is not the case since the synchronous solution is marginally stable. This can be shown by reasoning as for the evaporation exponent. Let us imagine feeding a neuron characterized by a leaky current $\tilde{a}$ with the train of spikes emitted by a network of identical synchronous neurons (characterized by the current a). Such a train is nothing but a series of truncated exponentials that repeat themselves after a self-determined period. Accordingly, one can apply the same arguments developed in Ref. [10] for the TMS model: While for $\tilde{a} < a$ the single neuron locks to the periodic forcing, for $\tilde{a} > a$ there is no locking since there is no longer any fixed point (which disappears exactly for $\tilde{a} = a$, which is the reason for the asymmetric stability of the synchronous solution). Strictly speaking, in the present context all neurons are identical and thereby affected by the same leaky current; however, the

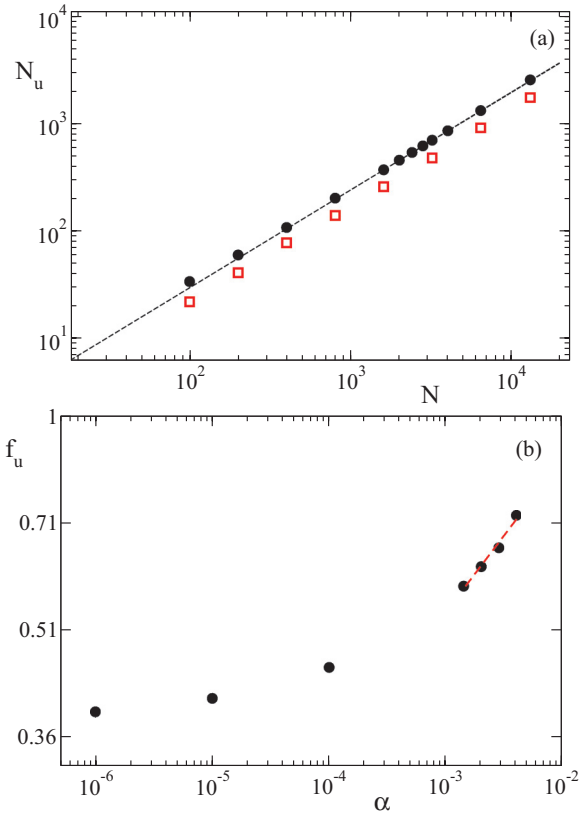

FIG. 7. (Color online) (a) Diluted networks: number of unlocked neurons N_u as a function of the size N for a network with short-term plasticity (black circles) and for a network with exponential pulse interactions (red open squares). The black dashed line is a power-law fit with exponent $\eta = 0.90 \pm 0.01$. (b) Inhomogeneous globally coupled network with exponential pulse interactions: f_u as a function of the width of the inhomogeneity in the leaky currents α for $N = 5000$ for the TMS model [10] (log-log scale). The red dashed line is a power-law fit with exponent $\zeta = 0.2 \pm 0.02$. To determine the number of unlocked neurons we have considered those neurons that do not belong to the plateau [see Fig. 6(b) for diluted network with short-term plasticity]. Finally, in both panels the measures have been averaged over five different realizations of the disorder (the corresponding error bars are smaller than the symbols).

disorder in the connections implies that the coupling term is, on average, different for the different neurons, which can be interpreted as an effective contribution to the leaky current. In fact, we have already seen in Fig. 6(b) that the effective connectivity is a meaningful parameter for the classification of the neuron behavior. It is interesting to note that for a much larger disorder [see the bottom curve in Fig. 6(b)], there exists a second unlocking transition. This is quite a standard phenomenon: The critical connectivity lies at a finite distance from the self-selected value that generates the frequency of the QSE and can be reached only for a large enough disorder.

More than just observing $f_u \neq 0$ for any amount of disorder, in Ref. [10] it was found that f_u remains finite even when the disorder vanishes (although the average frequency separation vanishes as well). Given the difference between the TMS model and the setup studied in this paper, we have further explored both models. We started determining f_u in the TMS model for a flat distribution of leaky currents (which covers the interval $[a - \alpha; a + \alpha]$, as in Ref. [10]). The results plotted in Fig. 7(b) show that f_u indeed saturates (see, however, the horizontal logarithmic scale). In contrast, if one restricts the analysis to α values between 10^{-2} and 10^{-3} one finds an effective power-law decay with an exponent $\zeta = 0.2 \pm 0.02$ [see Fig. 7(b)]. Notice that this result is consistent with the scaling observed in our model, where the disorder amplitude of the TMS model α has to be replaced by a function that scales as $N^{1/2}$. This suggests that the scaling behavior reported in Fig. 7(a) could be a finite-size effect. However, it is important to note that one should need unreasonably large network sizes ($\approx 10^{10}$) to observe a saturation effect that sets in at such small noise amplitudes (around 10^{-5}). Accordingly, even if the power-law decay were to be restricted to a finite range of connectivities, it would be a relevant effective phenomenon in the context of realistic neural networks.

In order to shed further light on this delicate issue, we have investigated yet another setup, namely, a diluted network of identical LIF neurons with exponential postsynaptic potentials, adjusted in such a way that their decay time coincides with the time constant τ_{in}. In other words, this last model differs from the one studied throughout this paper only for the absence of the synaptic plasticity. The corresponding results, reported in Fig. 7(a) (open squares), are quite close to those obtained for the original model. The nice agreement has a twofold consequence. First, it confirms that the scaling behavior exhibited by f_u is a sufficiently general and robust phenomenon. More than that, the power-law decay is rather clean (it covers two decades). In order to have some additional hints as to whether the network disorder is fully captured by the neuron connectivity, we performed yet other simulations where each neuron has been forced to have the same number of synaptic connections, so that the disorder is only hidden in the topology of the network structure. Simulations performed for different network sizes (not reported) have shown that the splitting of neurons into two blocks of locked and unlocked neurons is still present. This suggests that there is more to be learned by investigating the topological structure of the network. The second implication of the agreement between the two data sets reported in Fig. 7(a) is that short-term synaptic plasticity is equivalent (for these parameter values) to assuming an exponential shape for the synaptic pulses. In fact, the variable z, being characterized by a small decay rate τ_r, exhibits rather small oscillations (see, for instance, Fig. 4) and thereby plays a limited role. Since the ratio between τ_{in} and τ_r has been fixed to match the phenomenological observations, one can conclude that a crucial condition for the short-term plasticity to give rise to entirely new phenomena is that of slowing down the spiking frequency. This could be obtained, for instance, by assuming that the leaky current a is close to the threshold value ($a = 1$).

V. EFFECT OF NOISE

In the preceding sections we have discussed the emergence of QSEs in the deterministic evolution of a diluted network of LIF neurons with excitatory coupling in the presence of short-term plasticity. This dynamical regime is characterized

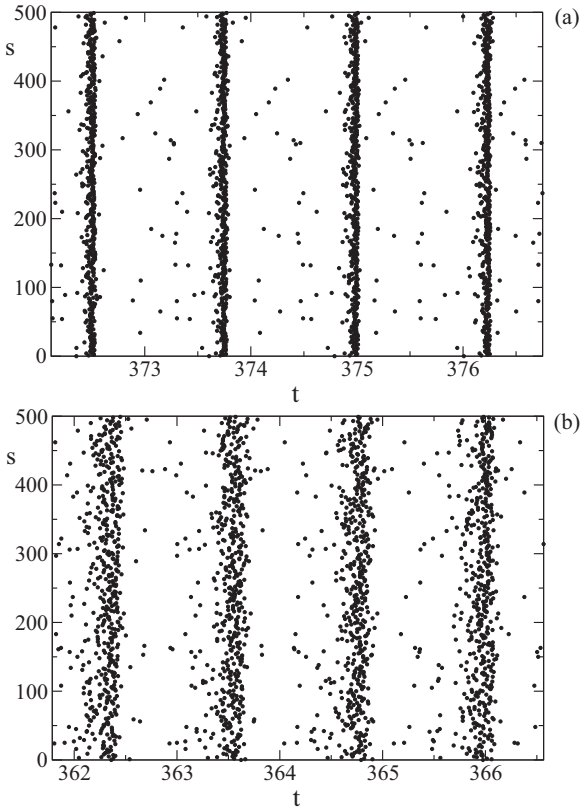

FIG. 8. Firing patterns of the stochastic dynamics in the case of noise on the reset potential for a diluted network with $N = 500$, $\tau_{in} = 0.2$, and different noise amplitudes (a) $\Delta = 0.05$ and (b) $\Delta = 0.15$. We indicate with s the index of the neuron firing at time t.

by a weak level of chaos, which is expected to vanish in the thermodynamic limit, when the mean-field dynamics fully sets in. This is quite an interesting result since QSEs appear without the need of any stochastic components as in previous studies [1,2,6,7,9]. It is nevertheless reasonable to expect that a neural network should be affected by some level of noise as a product of endogenous ionic- and synaptic-current fluctuations or of external sources. For this reason, in this section we investigate the effect of different forms of stochastic noise.

As a first case study we consider the action of noise on the value of the membrane reset potential, which could be attributed to uncorrelated fluctuations of extracellular and intracellular ionic concentrations. This amounts to modifying the event-driven algorithm described by Eqs. (10)–(12) by randomly selecting the reset potential ξ_n within the interval $[-\Delta, \Delta]$ according to a uniform distribution. As a result, the number of unlocked neurons increases with respect to the deterministic evolution. The higher the noise amplitude, the larger this group of neurons is. Nonetheless, QSEs are still present, even for quite high noise amplitudes (see Fig. 8).

A quantitative analysis can be performed by studying global variables. In Fig. 9 we compare the dependence of the Kuramoto parameter on τ_{in} in the deterministic and the noisy cases ($\Delta = 0.05$). The two plots are quite close to each other, except for the transition region (from the partially synchronized phase to the asynchronous one). As expected, noise is found to shift the transition point to a lower value

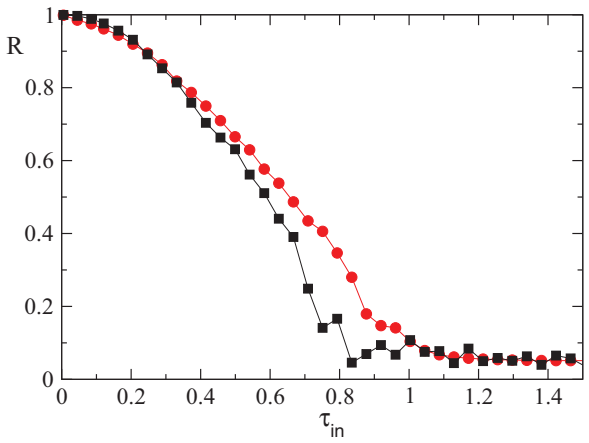

FIG. 9. (Color online) Kuramoto order parameter R as a function of τ_{in} in a diluted network with $N = 500$ for deterministic dynamics (red circles) and stochastic dynamics in the case of noise on the reset potential with $\Delta = 0.05$ (black squares). The values of R have been obtained by averaging over a temporal length of 4,000 after discarding a transient of $1000N$ iterations of the map.

of the control parameter τ_{in}. The evolution of the synaptic fields $Y(t)$ and $Z(t)$ is also modified by noise (see Fig. 10), although it remains close to the deterministic attractor. A major change is the increase of the transversal width, which signals larger amplitude fluctuations. In Fig. 5 we have plotted the distribution of T_q; the effect of the noise is to shift it to smaller values and to increase the variance with respect to the deterministic case.

Noise can be introduced into the event-driven map (11) also by adding a stochastic contribution $\xi_i(n)$ to the leaky current

$$a_i(n) = \bar{a} + \xi_i(n), \tag{18}$$

where $\bar{a}$ is the average value and ξ_i are randomly and uniformly distributed in the interval $[-\Delta, \Delta]$. In practice, after the last firing event in the network, $a_i(n)$ changes according to the stochastic rule (8) and then one can compute, as usual, the next-

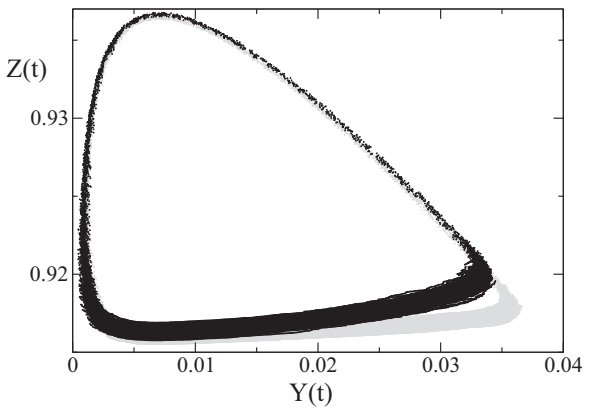

FIG. 10. Comparison between the global attractors for the deterministic dynamics (gray curve) and the stochastic dynamics in the case of noise on the reset potential (black curve). Both attractors have been obtained for the same diluted network with $N = 500$ and $\tau_{in} = 0.2$; data are reported after discarding a transient of $1000N$ iterations of the map; the noise amplitude of the stochastic dynamics has been set to $\Delta = 0.05$.

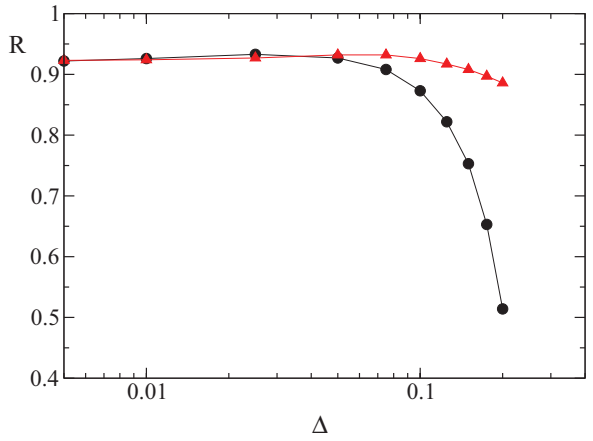

FIG. 11. (Color online) Kuramoto order parameter R as a function of the noise amplitude Δ in a diluted network for the two different kinds of stochastic dynamics: black circles and red triangles refer to noise on the reset potential and on the leaky current, respectively. The values of R have been obtained by averaging over a temporal length of 40 000 after discarding a transient of $1000N$ iterations of the map. The parameters are $\tau_{in} = 0.2$ and $N = 500$.

to-fire neuron as well as its firing time. Once again QSEs are robust against the addition of this form of noise. The statistics of T_q is still Gaussian and characterized by a smaller variance (typically $\sigma \sim 4 \times 10^{-3}$) with respect to the case of reset noise for the same value of Δ (see Fig. 5).

Finally, in Fig. 11 we show the dependence of the Kuramoto parameter R on the noise amplitude Δ for both noise forms. In both cases R decreases when Δ increases; the phenomenon is stronger in the case of the reset noise. However, Fig. 11 shows that even for high amplitudes of Δ, the dynamics is characterized by a partially synchronized phase, as in the deterministic case. From these analyses we can conclude that the QSE phase observed in the deterministic model is robust against the presence of even relatively strong stochastic components.

Notice that the average value $\bar{a}$ of the leaky current is an important parameter, as it controls the average ISI as well as $\langle T_q \rangle$. In this section we have assumed $\bar{a} = 1.3$ (as in the deterministic case). A value of $a < 1$ means that the neuron is below threshold and cannot fire by itself. However, in the presence of a stochastic dynamics $\bar{a} < 1$ and yet fluctuations may occasionally induce the firing of some neurons, which in turn may trigger avalanches of many other neurons. Altogether, QSEs may still occur, although with a much smaller frequency. By choosing $\bar{a} = 0.9$ and $\Delta = 0.15$, we have found that $\langle T_q \rangle$ is of the order of a few seconds in physical units, a value that is very close to the one observed in Ref. [2], where quenched disorder was attributed to the leaky current. In practice, we have analyzed the annealed version of this model, showing that quenched and annealed noise yield rather similar results. An important consequence of our study is that the PBs analyzed in Ref. [2] have the same dynamical origin as the QSEs analyzed in this paper, although large values of T_q can be observed only in the presence of a large fraction of subthreshold neurons in a stochastic dynamics. In Ref. [2] this was a direct consequence of the high level of dilution of the network and the presence of a finite fraction of inhibitory neurons. In our annealed formulation this dynamical regime can be observed by selecting $\bar{a}$ sufficiently below 1.

VI. CONCLUSIONS AND OPEN PROBLEMS

The search for synchronous or quasisynchronous states in models of neural networks is a hot topic, mostly inspired by experimental studies that revealed the emergence of such behavior (see, e.g., Ref. [1]). In the past decade, several authors tackled this problem by making use of models that contain many different ingredients, such as LIF or Morris-Lecar neurons, diluted or globally coupled networks, quenched disorder, and stochastic components [1,2,6,7,9]. All of these models contain short-term plasticity, as it was initially conjectured [2] that it is a crucial ingredient for reproducing quasisynchronous evolution in a neural network. It was nevertheless unclear which minimal ingredients are really necessary to generate a dynamical phase characterized by highly synchronous events in the form of population bursts emitted by a large number of neurons.

In this paper we have shown that a randomly diluted neural network of LIF excitatory neurons equipped with short-term plasticity can exhibit QSEs in the absence of any stochastic component in the dynamics. Upon varying the decay time τ_{in} of the synaptic active transmitters, we observe a crossover from a QSE dynamical phase to an asynchronous regime. In the QSE phase neurons self-organize into two main groups: locked and unlocked neurons, primarily (but not exclusively) on the basis of their synaptic connectivity. In contrast, we have found that such QSEs can be reproduced by yet a simpler model, where synaptic plasticity is replaced by the emission of standard exponential pulses. Anyway, such events still differ from the population bursts observed experimentally. For instance, the statistics of the interburst events is purely Gaussian without the long time tails observed in Ref. [1]. This observation opens the problem of understanding which additional ingredient needs to be included to ensure better agreement.

On a theoretical ground, an important result of our study is the observation of unlocked neurons for arbitrarily small disorder (large networks). More precisely, the fraction of unlocked neurons decays as $N^{-0.1}$ and it is an open question whether such a slow decay saturates in the thermodynamic limit. Altogether, the scenario differs from the one observed in the Kuramoto model since the spontaneously generated synchronized component is marginally stable, i.e., it is unstable against an arbitrarily small increase of the leaky current. This is one of the many subtle phenomena that spontaneously emerge in massively coupled oscillators, such as the appearance of a robust quasiperiodic behavior in LIF neurons, where the frequency of the periodic collective motion adjusts itself to avoid any locking with the single-neuron dynamics [12].

Finally, we wish to comment on the scaling behavior of the maximum Lyapunov exponent. Let us start by observing that the locked neurons are expected to contribute only as slaved variables, i.e., to the negative part of the Lyapunov spectrum, and the same holds for the synaptic variables that are characterized by a relaxation dynamics. As a result, the variables that can actively contribute to the chaotic dynamics are just the phases of the unlocked neurons, which are of

the order of N_u. These arguments are confirmed by looking at the spectrum displayed in Fig. 3(a), where the number of nearly zero (both positive and negative) Lyapunov exponents (12) equals that of the unlocked neurons. More than that, one can see in the inset of the figure that the initial part of the spectrum is symmetric with respect to the zero axis, as in Hamiltonian systems. This is not a novelty in the context of weakly coupled phase oscillators. It has been observed, for instance, in Refs. [19,20] and traced back to the invariance of the dynamical equations under time reversal. Here it is not easy to prove time reversibility, as it seems to apply to a subset of variables. Therefore, we limit ourselves to infer the presence of a pseudo-Hamiltonian dynamics on the basis of a symmetric Lyapunov spectrum. In weakly coupled Hamiltonian systems, it is known that the maximal Lyapunov exponent λ_1 scales to zero as a power of the coupling strength ε ($\lambda_1 \approx \varepsilon^{\beta}$). The exponent β is equal to either $2/3$ or $1/2$, depending on whether the coupling term has zero average or not [21]. In our model, the coupling is induced by the statistical fluctuations of the last term in Eq. (9), i.e., $\varepsilon \approx \sqrt{N^{0.9}}/N = N^{-0.55}$. Moreover, since the coupling induced by the pulse emission modifies the average frequency of the oscillators, it is natural to expect that our model belongs to the latter universality class. Accordingly, one finds that $\lambda_1 \sim N^{-0.275}$, a behavior that is remarkably close to the numerical observations. However, this relationship deserves further theoretical investigation since it is based on an unproven analogy between weakly coupled unlocked LIF neurons and effective Hamiltonian systems.

ACKNOWLEDGMENTS

We wish to thank Arkady Pikovsky and Yuri Maistrenko for useful discussions. Partial support was provided by the Italian MIUR-PRIN Project No. 20083C8XFZ, the Joint Italian-Israeli Laboratory on Neuroscience funded by the Italian Ministry of Foreign Affairs, and the European Commission through the Marie Curie Initial Training Network "NETT" Project No. 28914.

APPENDIX: STABILITY OF THE SYNCHRONOUS STATE

In this Appendix we perform the stability analysis of the synchronous state in a globally coupled network of size N. By integrating the dynamical equations over one period τ, one obtains implicit equations that allow determination of τ and the synaptic variables $\tilde{y}$ and $\tilde{z}$ immediately after the firing event,

$$ae^{-\tau} = a + g\frac{\tau_{\rm in}}{\tau_{\rm in}-1}(e^{-\tau/\tau_{\rm in}} - e^{-\tau})\tilde{y} - 1, \tag{A1}$$

$$\tilde{y} = \tilde{y}e^{-\tau/\tau_{\rm in}} + u(1-\tilde{z}-\tilde{y}e^{-\tau/\tau_{\rm in}}), \tag{A2}$$

$$\tilde{z} = \tilde{z}e^{-\tau/\tau_r} + \frac{\tau_r}{\tau_r-\tau_{\rm in}}\tilde{y}(e^{-\tau/\tau_r} - e^{-\tau/\tau_{\rm in}}). \tag{A3}$$

We now determine the evaporation exponent by estimating how the potential of a probe neuron, forced by the mean field generated by a network, converges towards the synchronized state. The membrane potential of each neuron follows the evolution equation

$$\dot{v}(t) = a - v(t) + gY(t). \tag{A4}$$

For the probe neuron, the synaptic activity $Y(t)$ is to be considered as a periodic nonautonomous forcing. The stability analysis will be performed by following the evolution of the distance between the probe neuron and the synchronized cluster. Let us consider an initial condition where the potential of the network neurons has just been reset ($v_j = 0$), while the probe neuron is lagging behind [$v(0) = 1 - \delta(0)$]. The time s needed by the probe neuron to reach the threshold (i.e., the temporal distance from the synchronized cluster) is implicitly given by the condition

$$[1-\delta(0)]e^{-s} + a(1-e^{-s}) + \frac{g\tau_{\rm in}}{\tau_{\rm in}-1}(e^{-s/\tau_{\rm in}} - e^{-s})\tilde{y} = 1. \tag{A5}$$

Over the time s, the potential of the network neurons increases from 0 to

$$\begin{aligned}\delta(s) &= a(1-e^{-s}) + g\frac{\tau_{\rm in}}{\tau_{\rm in}-1}(e^{-s/\tau_{\rm in}} - e^{-s})\tilde{y} \\ &= 1 - [1-\delta(0)]e^{-s},\end{aligned} \tag{A6}$$

which represents the distance when the probe-neuron potential has been reset as well. From Eq. (A4) it then follows that

$$\dot{\delta} = -\delta, \tag{A7}$$

so that

$$\delta(\tau) = \delta(s)e^{s-\tau} \tag{A8}$$

and the evaporation exponent is

$$\Lambda = \lim_{\delta(0)\to 0} \ln\left[\frac{\delta(\tau)}{\delta(0)}\right] = \ln\left[\frac{a+g\tilde{y}}{a+g\tilde{y}-1}\right] - \tau. \tag{A9}$$

By obtaining τ and $\tilde{y}$ from Eqs. (A1), (A2), and (A3) one can estimate Λ. The dependence of the evaporation exponent on $\tau_{\rm in}$ is plotted in Fig. 12 (see the bottom curve). If one started

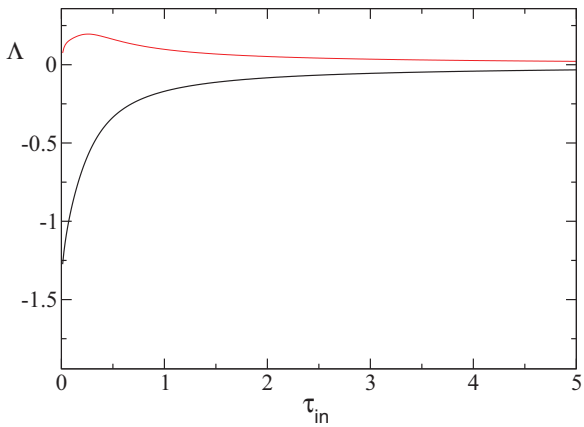

FIG. 12. (Color online) Evaporation exponents Λ as a function of $\tau_{\rm in}$: The bottom (black) curve and the top (red) curve refer to the left [see Eq. (A9)] and right exponents, respectively. We have used the following rescaled parameters: $g = 21$, $u = 0.5$, $a = 1.3$, and $\tau_r = 133\tau_{\rm in}$.

by assuming that the single neuron is ahead of the cluster, a different exponent would be obtained (see the top curve in Fig. 12, it corresponds to numerical evaluation of the right exponent but it's possible to obtain also an analytical formula with calculations similar to those used for the left exponent): The meaning of this phenomenon is discussed in the main text.

The behavior for small τ_{in} is somehow surprising since, as shown in Sec. III, the effect of the coupling tends to vanish for $\tau_{\text{in}} \to 0$. In order to clarify this point, we perform a perturbative analysis. From Eqs. (A1), (A6), and (A8), under the assumption of τ_{in} and $\delta(0)$ small, one finds

$$\delta(\tau) = \frac{a-1}{a}[\delta(0) + s]. \tag{A10}$$

At the same time, Eq. (A5) reduces to

$$s(a-1) + a\tilde{y}\tau_{\text{in}}(1 - e^{-s/\tau_{\text{in}}}) = \delta(0). \tag{A11}$$

If $s \ll \tau_{\text{in}}$, we are in the regime of infinitesimal perturbations; the exponential in the above equation can be expanded, giving rise to

$$s = \frac{\delta(0)}{a - 1 + g\tilde{y}}. \tag{A12}$$

By replacing in Eq. (A10) one finally obtains

$$\frac{\delta(\tau)}{\delta(0)} = \frac{(a-1)(a+g\tilde{y})}{a(a-1+g\tilde{y})}. \tag{A13}$$

The logarithm on the right-hand side is just the evaporation exponent for $\tau_{\text{in}} = 0$. If instead $\tau_{\text{in}} \ll s$, the exponential in Eq. (A11) can be neglected, giving rise to

$$s = \frac{\delta(0) - g\tilde{y}\tau_{\text{in}}}{a-1}. \tag{A14}$$

Again with the help of Eq. (A10) one obtains

$$\delta(\tau) = \delta(0) - \frac{g}{a}\tilde{y}\tau_{\text{in}}. \tag{A15}$$

Equations (A13) and (A15) tell us that whenever the time separation s between the probe neuron and the cluster is larger than the decay time τ_{in} the physical distance decreases linearly in time with a coefficient that becomes increasingly small with τ_{in}. However, as soon as the distance becomes on the order of τ_{in}, an exponential convergence sets in that is ruled by an exponent that remains finite even for arbitrarily small τ_{in} values.

[1] V. Volman, I. Baruchi, E. Persi, and E. Ben-Jacob, Physica A **335**, 249 (2004).
[2] M. Tsodyks, A. Uziel, and H. Markram, J. Neurosci. **20**, RC50 (2000).
[3] M. Tsodyks and H. Markram, Proc. Natl. Acad. Sci. USA **94**, 719 (1997).
[4] M. Tsodyks, K. Pawelzik, and H. Markram, Neural Comput. **10**, 821 (1998).
[5] C. Morris and H. Lecar, Biophys. J. **35**, 193 (1981).
[6] E. Fuchs, A. Ayali, E. Ben-Jacob, and S. Boccaletti, Phys. Biol. **6**, 036018 (2009).
[7] C.-C. Chen and D. Jasnow, Phys. Rev. E **84**, 031908 (2011).
[8] R. Brette, Neural Comput. **18**, 2004 (2006).
[9] A. Morrison, A. Aertsen, and M. Diesmann, Neural Comput. **19**, 1437 (2007).
[10] M. Tsodyks, I. Mitkov, and H. Sompolinsky, Phys. Rev. Lett. **71**, 1280 (1993).
[11] R. Zillmer, R. Livi, A. Politi, and A. Torcini, Phys. Rev. E **76**, 046102 (2007).
[12] C. van Vreeswijk, L. F. Abbott, and G. Bard Ermentrout, J. Comp. Neurosci. **1**, 313 (1994); C. van Vreeswijk, Phys. Rev. E **54**, 5522 (1996).
[13] D. Hansel, G. Mato, and C. Meunier, Neural Comput. **7**, 307 (1995).
[14] A. Pikovsky, O. Popovych, and Yu. Maistrenko, Phys. Rev. Lett. **87**, 044102 (2001).
[15] Y. Kuramoto, *Chemical Oscillations, Waves, and Turbulence* (Dover, New York, 2003).
[16] J. A. Acebrón, L. L. Bonilla, C. J. Peréz Vicente, F. Ritort, and R. Spigler, Rev. Mod. Phys. **77**, 137 (2005).
[17] S. Olmi, R. Livi, A. Politi, and A. Torcini, Phys. Rev. E **81**, 046119 (2010).
[18] L. Tattini, S. Olmi, and A. Torcini, Chaos **22**, 023133 (2012).
[19] D. Topaj and A. Pikovsky, Physica D **170**, 118 (2002).
[20] S. A. Marvel, R. E. Mirollo, and S. H. Strogatz, Chaos **19**, 043104 (2009).
[21] G. Paladin and A. Vulpiani, J. Phys. A **19**, 1881 (1986).